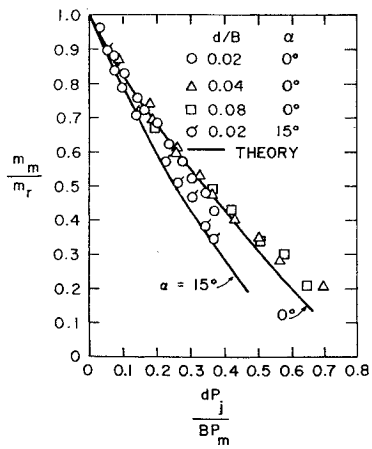

Fig. 2 Experimental results.

credible when applied to regions near the base of the jet where stagnation conditions are to be expected. By defining a pressure weighting function, it was found that the results of the analysis were insensitive to the assumption that mainstream static pressure acts at all points along the jet face. In retrospect, this result could be expected since, for large jet penetrations, the throttling effect reduces mainstream velocities near the point of injection to values that lead to small differences between static and stagnation pressures.

Application of mass continuity in the mainstream allows an exchange of the mainstream Mach number, M, for the height y in Eq. (3) (see Ref. 1 for details). The result is

$$C = \frac{B}{d}\frac{P_m}{P_j}\int_{M_{mo}}^{1} \pi(M)\frac{A(M)}{A(M_{mo})}\left(\frac{1}{M} - \frac{[(\gamma+1)/2]M}{1+[(\gamma-1)/2]M^2}\right)dM \tag{4}$$

where $\pi(M)$ and $A(M)$ are the familiar Mach number functions for pressure ratio (p_m/P_m) and area ratio (A/A^*) in locally isentropic flow. With specified values for $C(B/d)(P_m/P_j)$, Eq. (4) is easily solved for M_{mo}.

The throttling effect of the jet is given by

$$m_m/m_r = 1/A(M_{mo}) \quad \text{and} \quad m_j/m_r = (d/B)P_j/P_m \tag{5}$$

Data were obtained[1] for values of d/B in the range 0.02 to 0.08 and for P_j/P_m from 2 to 20. The experiments utilized air flows under conditions such that the jet was sonic at injection Results for $\alpha = 0°$ and 15° are shown in Fig. 2. The analysis accurately predicts the measured flow rates for conditions in which the mainstream is reduced to approximately 40% of its unthrottled value. For conditions of upstream injection, the agreement with experiment should be given only qualitative credence since in the experiments the actual angle of injection was difficult to determine. The deviation of theory from experiment at very large injection rates is thought to be due mainly to the neglect of viscous effects.

References

[1] Frick, K., "Jet Penetration and Interaction at a Sonic Throat," thesis (AD743079), March 1972, Naval Postgraduate School, Monterey, Calif.

[2] Nunn, R. H. and Brandt, H., "Aerodynamic Throttling of Two-Dimensional Nozzle Flows," *The Aeronautical Quarterly*, Vol. 23, Feb. 1972, pp. 53–61.

[3] Barnes, J., Davis, J., and Tang, H., "Control Effectiveness of Transverse Jets Interacting with a High-Speed Free Stream," AFFDC-TR-67-90, Vol. I, Sept. 1967, Air Force Flight Dynamics Lab., Dayton, Ohio.

Turbulent Interference Heating on Several Small Fin Configurations

HUGH W. COLEMAN* AND E. CLARK LEMMON*
Sandia Laboratories, Livermore, Calif.

Nomenclature

Q = heating rate
M = Mach number
Re = Reynolds number

Subscripts
c = conditions on the cone at the fin station
e = boundary-layer edge at the fin station
x = surface distance on the cone
LE = conditions on the stagnation line of the fin leading edge

Introduction

WHEN aerodynamic control fins are used on high velocity vehicles, regions of increased heating occur on the vehicle surface in the vicinity of the fin and also on the body of the fin itself. The flowfield in such regions is complex and does not yield itself to a straightforward analytical description. It is therefore necessary to investigate this type of problem experimentally. This Note presents turbulent heating distributions measured in the interference region on and around several small, highly-swept fin configurations mounted on a cone.

Test Program

The tests were conducted in the LTV Aerospace Corp.—Vought Aeronautics Div. High Speed Wind Tunnel over a range of freestream Mach numbers from 2.71 to 4.97 and freestream Reynolds numbers from 1.1 to 2.8 × 10^7/ft. The 3-in. long fins were mounted on the aft end of a 6° half-angle, 10-in. base diameter cone. Two noses were used, one sharp and one 40% blunt, to vary local flow conditions on the fins. Boundary-layer thicknesses were about one-third the fin height and no evidence of separation was observed. Heat-transfer data were obtained on the fins and in the interference region on the cone using the transient thin skin technique. A complete description of the test program and results is given in Refs. 1 and 2. The results for the fin leading edge stagnation line were analyzed and discussed in Ref. 3.

Results

The experimental heat-transfer distributions around the leading edge and along the side of several 60° swept, cylindrical leading edge fins are shown in Fig. 1. The data represent a range of local Mach numbers, M_e, from 2.13 to 4.71 and local Reynolds numbers, Re_x, from 1.4 to 11.0 × 10^7. The heating rate decreases around the leading edge to about 40%–60% of the stagnation line value at the tangency point and decreases further to about 20%–45% along the fin side. A comparison of these data with the prediction obtained using the expression of Beckwith and Gallagher[4] for the turbulent circumferential heating for a 60° swept cylinder in a freestream with a Mach number range from 4.71 to 2.13 is given in Fig. 1. The comparison indicates that the data on the fin face forward of the tangency point generally lie above the prediction range.

Received June 4, 1973; revision received August 3, 1973. This work was supported by the U.S. Atomic Energy Commission under Contract AT-(29-1)-789.

Index categories: Boundary Layers and Convective Heat Transfer —Turbulent; LV/M Aerodynamic Heating.

* Member of Technical Staff, Aerothermodynamics Division.

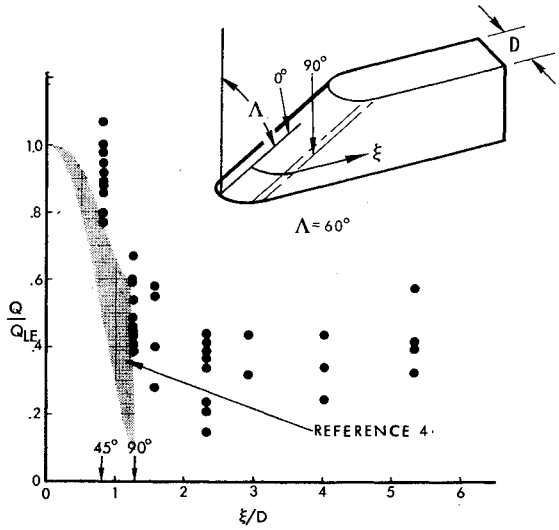

Fig. 1 Heating distribution around the leading edge and along the side of cylindrically faced fins.

The effect of leading edge geometry is shown in Fig. 2, where the heating distribution on a 60° swept fin with a flat leading edge and rounded corners is presented. The data are for the same Mach number range as above and Re_x from 1.5 to 7.2 × 10^7. Comparison of these data with those of Fig. 1 shows a slightly different distribution around to the tangency point, with the heating levels on the fin sides approximately the same.

The heating distribution in the corner region formed by the intersection of the fin side and the cone surface was also determined for the configuration of Fig. 1. Figure 3 shows the heat-transfer data from this region nondimensionalized by the undisturbed cone heating at the fin station. The heating on the cone surface decreases away from the corner. In the immediate region of the corner the heating on the fin side is less than that in the corresponding area on the cone. The maximum heating observed in the corner region was about 2½ times the undisturbed cone value.

Figure 4 presents data on an entirely different configuration, a split fin with a stationary forward section and a movable aft section. Heating data were obtained with the aft section at 0° and 15° cant and are shown normalized by undisturbed

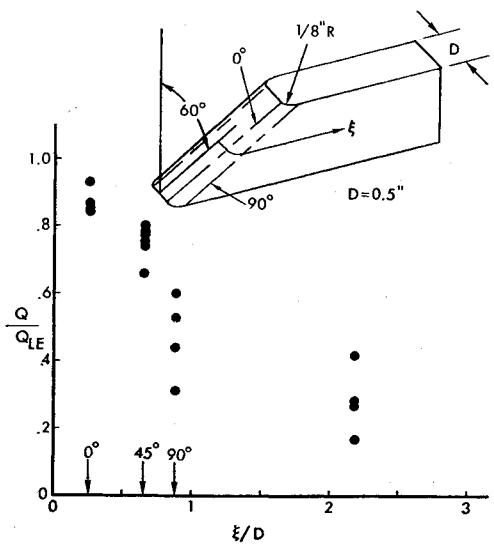

Fig. 2 Heating distribution around the leading edge and along the side of a flat faced fin.

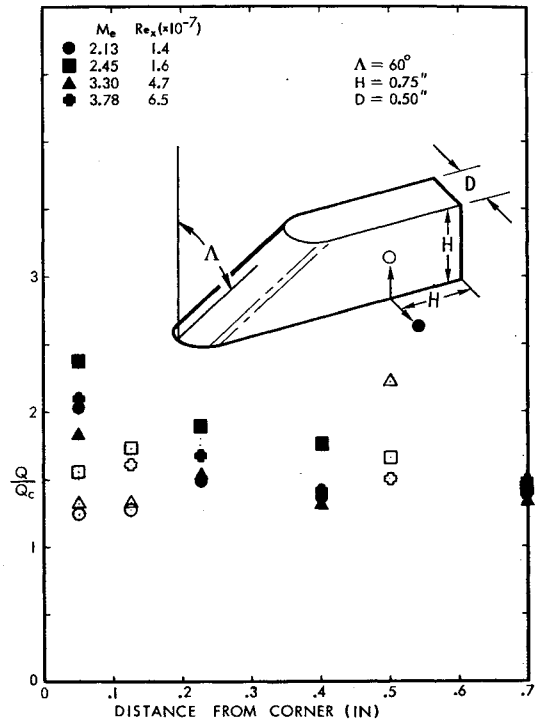

Fig. 3 Corner heating distribution for 60° swept, cylindrically faced fin.

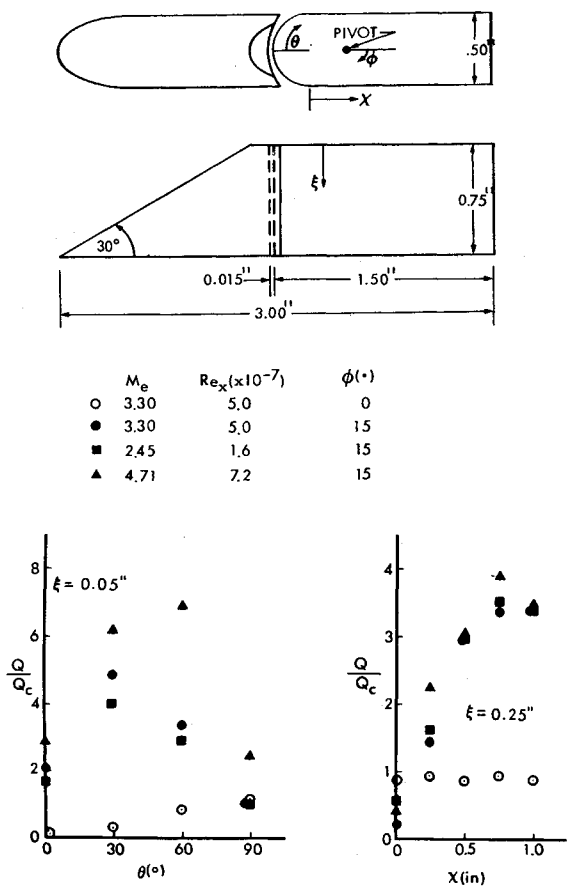

Fig. 4 Heating distribution on a split fin configuration for 0° and 15° cant.

cone heating for convenience. The cylindrical front portion of the movable section experiences quite severe heating at the 15° cant position due to reattachment of the flow off the forward section of the fin. Values up to seven times cone heating were measured. The heating along the windward side of the canted aft section increases along its length to a maximum of three and a half to four times the uncanted value. This value exhibits only a very weak dependence on flow conditions.

References

[1] Coleman, H. W. and Lemmon, E. C., "Turbulent Heat Transfer and Pressure on Leading Edges of Fins Mounted on a Cone," SCL-RR-720308, 1972, Sandia Labs., Livermore, Calif.

[2] Coleman, H. W. and Lemmon, E. C., "Turbulent Heat Transfer and Pressure in the Interference Region of Fins Mounted on a Cone," SCL-RR-720309, 1973, Sandia Labs., Livermore, Calif.

[3] Coleman, H. W. and Lemmon, E. C., "The Prediction of Turbulent Heat Transfer and Pressure on a Swept Leading Edge Near Its Intersection With A Vehicle," AIAA Paper 73-677, Palm Springs, Calif., 1973.

[4] Beckwith, I. E. and Gallagher, J. J., "Local Heat Transfer and Recovery Temperatures on a Yawed Cylinder at a Mach Number of 4.15 and High Reynolds Numbers," TR R-104, 1958, NASA.

Modeling Sublimation of a Charring Ablator

JOHN F. BALHOFF* AND RALPH W. PIKE†
Reacting Fluids Laboratory, Louisana State University, Baton Rouge, La.

Nomenclature

A = area
C_i = mass fraction of species i
J_i = diffusive mass flux
$\bar{M}$ = average molecular weight
M_i = molecular weight of species i
m_i = mass flux of species i
P = pressure
P_{vap} = vapor pressure
R = gas constant
T = absolute temperature
v = velocity
α_i = accommodation coefficient of species i
ω_i = reaction rate of species i
ρ = density
ε = porosity

Introduction

THE determination of the sublimation rate of carbon for a char forming ablative heat shield is necessary to fully describe the material response to aerodynamic heating. This sublimation rate is required in the surface mass and energy balances which give the interaction of the flowfield and the ablator.

The sublimation model that is used in this analysis and compared to other investigators is based on the Hertz-Knudsen equation. The basic equation originally given by Hertz in 1882[1] relates in the mass of molecules striking a unit area per unit time to the pressure and temperature of the gas. The theoretical model is shown to compare quite favorably with arcjet experimental data and demonstrates its usefulness by its accuracy and simplicity.

Model Description

For nonequilibrium such as the case where the subliming material is continually removed, the net rate of evaporation is given by the well-known Hertz-Knudsen equation[2]

$$\dot{m} = \alpha(A_r/A)(M/2\pi RT)^{\frac{1}{2}}(P_{vap} - P) \quad (1)$$

The preceding equation can be extended for vaporization of a solid into a mixture of gases by replacing the total pressure, P, with partial pressure of the vaporizing component, P_i

$$\dot{m}_i = \alpha_i(1-\varepsilon)(M_i/2\pi RT)^{\frac{1}{2}}(P_{i,vap} - P_i) \quad (2)$$

For subliming carbon i refers to C_1, C_2, and C_3 vapor. The effective area ratio A_r/A is approximated by $(1-\varepsilon)$ where ε is the char porosity.

Carbon Species

Studies[3] have shown that the three primary constituents of subliming carbon are C_1, C_2, and C_3. These species have Arrhenius dependence of vapor pressure on temperature of the form $\log P_i = a_i + b_i/T$. The accommodation coefficients, α_i, along with the Arrhenius vapor coefficients[4] are given in Table 1.

Surface mass balance

The general species mass balance at the surface of the ablator includes convective flux to and away from the surface ($\rho v C_i$), diffusive flux to and away from the surface (J_i), and surface generation by chemical reaction (ω_i). The species mass balance is stated as follows:

$$\rho v C_i^- + \omega_i + J_i^- = \rho v C_i^+ + J_i^+ \quad (3)$$

In the region where the rate of sublimation is significant, surface chemical reactions and diffusion will not be important, and this is the case for the high heating rates encountered during manned return from planetary missions. The result is a porous char vaporizing into the gaseous species C_1, C_2, and C_3. Also flowing through this porous matrix is the pyrolysis gas from the decomposition zone of the ablator. In Ref. 5 there was an error in the nitrogen composition of the pyrolysis gas from a phenolic-nylon ablator, and correct values are reported in Table 2. Also reported in Table 2 is a typical composition of the pyrolysis gases at the ablator surface computed from a nonequilibrium char zone analysis described in Ref. 6, an extension of the work of Ref. 7. The analysis considers the pyrolysis gas from the decomposition zone flowing through the char zone and reacting at a finite rate.

Combining the Hertz-Knudsen equation, Eq. (2), with the surface mass balance for these previously described conditions for i being C_1, C_2, or C_3, the mass flux of these gaseous carbon species injected into the shock layer is given by

$$\rho v C_i^+ = \alpha_i(1-\varepsilon)(M_i/2\pi RT)^{\frac{1}{2}}(P_{i,vap} - P_i^+) \quad (4)$$

Table 1 Accommodation coefficients and Arrhenius coefficients for vapor pressure of C_1, C_2, and C_3 (Ref. 4)

Species	Accommodation coefficient, α_i	$\log P_{i,vap} = a_i - b_i \times 10^4/T$	
		a_i	b_i
C_1	0.37	8.14	3.72
C_2	0.34	9.69	4.23
C_3	0.08	9.81	4.03

Received June 28, 1973; revision received July 26, 1973. Support by NASA under Grant NGR-19-001-059 for this work is gratefully acknowledged.

Index categories: Material Ablation; Thermochemistry and Chemical Kinetics.

* Research Associate in Chemical Engineering.

† Professor of Chemical Engineering. Member AIAA.